THE ASTRONOMICAL JOURNAL VOLUME 108, NUMBER 2 AUGUST 1994

NEAR-INFRARED IMAGING SURVEY OF YOUNG STELLAR OBJECTS IN BOK GLOBULES

JOÃO LIN YUN
Departamento de Física, Universidade de Lisboa, Campo Grande, Ed. C1, 1700 Lisboa, Portugal

DAN P. CLEMENS
Department of Astronomy, Boston University, 725 Commonwealth Avenue, Boston, Massachusetts 02215

Received 1993 October 26

ABSTRACT

We performed a near-infrared imaging survey toward 34 Bok globules containing *IRAS* point sources, which were young stellar objects (YSOs) candidates. We used state-of-the-art NICMOS 3 and SQIID cameras for this survey. Visual examination of the images revealed that 20 globules showed evidence of nebular emission or very red stellar objects located at the position of the YSO candidates. The *IRAS* 12/25 μm spectral indices of these 20 objects are distinctively different from those of the 14 globules which showed no nebulosity, in the sense that more than 50% of the 20 nebular or very red objects have negative *IRAS* 12/25 μm spectral indices, while only 20% of the 14 non-nebular objects show such red *IRAS* colors. Analysis of the near-infrared nebulosities present in the images revealed the following: (1) these nebulosities generally contain a stellarlike source surrounded by an extended component; (2) several possible binaries with separations of about 10″ were found to reside in common infrared nebulosity; (3) infrared reflection nebulae, seen at 2.2 μm, are good tracers of CO mass outflow morphology. The group of objects displaying nebulosities, when ordered by their increasing 12/25 μm indices, seems to form an evolutionary sequence. Large negative 12/25 μm indices seem to indicate objects deeply embedded in their clouds (by showing nebulosities mostly in the *K* band, having associated molecular outflows, and no optical counterparts). As these objects reach later stages of their pre-main-sequence evolution (by showing nebulosity in the *J* band only, no detected molecular outflow, and having optical counterparts or optical nebulae), their 12/25 μm indices increase and become positive.

1. INTRODUCTION

Despite major, important progress in our knowledge of the star-formation process in the Galaxy, an endless number of questions, related to the central question "How do stars form?", remain to be answered. Star formation has been studied in the complex environments of giant molecular clouds where the very conspicuous massive star formation takes place. Star formation has also been studied in complexes of dark clouds where multiple episodes of star formation, possibly induced by young star activity, offer a complicated picture of the star-formation process. We were interested in learning whether stars form efficiently in the simpler environments of small molecular clouds and particularly in the simplest structures of the interstellar medium containing predominantly molecular hydrogen: the isolated, small Bok globules.

Bok globules are nearby small dark clouds of cold ($T_{\rm kinetic}\sim$10 K) gas and dust often containing small ($\sim$0.1 pc), dense ($n_{\rm H_2} \sim 10^4$ cm^{-3}) cores. Optically, they appear as isolated, dark, roundish patches of obscuration against the stellar background. They usually have well-defined edges and several magnitudes of visual extinction. They can be crudely separated into two broad classes: the large globules, with masses greater than $\approx$100 $M_\odot$ (e.g., B5; Young *et al.* 1982), and the small globules, with correspondingly smaller masses ($\approx$10 $M_\odot$; Clemens, *et al.* 1991).

As early as 1947, Bok suggested that globules were undergoing gravitational collapse on their way to form stars (Bok & Reilly 1947). However, until very recently, Bok's hypothesis remained untested.

Because of their small sizes, regularity, and isolation, globules can be convenient objects in which to study the formation of an individual star. The small globules are especially well suited, as they are the simplest clouds, with single, central condensations and little supersonic gas motion (e.g., Dickman & Clemens 1983). However, only a few studies of such Bok globules have been performed (cf. theory: Villere & Black 1980; observations: Leung, *et al.* 1982), with only a few clouds sampled. Furthermore, if stars form in Bok globules, they are likely to be low-mass stars, as the globules themselves have small masses. These stars are much less disruptive to their parent molecular cloud than massive stars (e.g., Zinnecker 1988). Thus, Bok globules should provide a more accurate picture of the physical conditions existing in small molecular clouds prior to, during, and just after the onset of star formation.

Since Bok & Reilly's (1947) conjecture, only a couple of small globules have been found to contain embedded infrared point sources (e.g., B335: Keene *et al.* 1983). In the last ten years, infrared, optical, and radio observations have provided other scattered evidence that low-mass stars form in Bok globules (Bok 1978; Frerking & Langer 1982; Reipurth 1983; Ogura & Hasegawa 1983; Goldsmith *et al.* 1984; Frerking *et al.* 1987; Cabrit *et al.* 1988; Moriarty-Schieven & Snell 1989; Sugitani *et al.* 1989; Duvert *et al.* 1990).

 0004-6256/94/108(2)/612/17/$0.90

However, no systematic, large-scale investigation of star formation in Bok globules has been performed.

In this paper, we describe the third part of such a study. The first and second parts were: (1) a search for embedded YSO candidates, performed by analyzing the mid-infrared emission detected by *IRAS* arising from the CB (Clemens & Barvainis 1988) sample of small Bok globules (Yun & Clemens 1990); (2) an outflow probe, in the ^{12}CO $J=1-0$ rotational line, of high-velocity molecular gas associated with the YSO candidates discovered in the previous work (Yun & Clemens 1992) with follow-up high-resolution mapping of the detected outflows (Yun & Clemens 1994a).

This paper describes the third part of our study, a new near-infrared (JHK) imaging survey of young stellar objects (YSOs) in many of the Bok globules already studied, and presents the results of a visual inspection of the images obtained. In particular, we present near-infrared isophote maps of regions of the globules containing the positions of YSO candidates where near-infrared nebulosity can be seen. These maps reveal the morphologies of these near-infrared nebulae and also reveal the presence of very "red" objects, that is, objects that are much brighter in the K band (2.2 μm) than in the J band (1.25 μm). The relationships between the *IRAS* 12/25 μm spectral indices of the YSO candidates, the near-infrared nebulosities and the presence of outflows, as well as the presence of optical nebulosity, are explored and discussed. We conclude that these YSO candidates in Bok globules are *bona fide* YSOs and that star formation is a rather common event in these globules.

In the fourth part of this study (Yun & Clemens 1994b), we will present the photometry of all red stellar objects found here, as well as their broadband spectral energy distributions, and will discuss their evolutionary states.

2. OBSERVATIONS AND DATA REDUCTION

The near-infrared (J, H, and K bands, i.e., $\lambda=1.25$, 1.65, and 2.2 μm) survey of YSO candidate sources was carried out during two observing periods. The first took place in 1991 May using the University of Arizona NICMOS 3 array camera (Rieke *et al.* 1989; Thompson *et al.* 1989) on their Mount Bigelow 1.5 m telescope. The second observing period was conducted in 1991 November using the Kitt Peak National Observatory Simultaneous Quad Infrared Imaging Device, SQIID camera (Ellis *et al.* 1992) on their 1.3 m telescope.

2.1 NICMOS 3 Data

During 1991 May 22–27, we used the University of Arizona NICMOS 3 infrared array to obtain J, H, and K band images towards 15 Bok globules: CB 81, CB 87, CB 90, CB 128, CB 141, CB 171, CB 180, CB 188, CB 203, CB 205, CB 206, CB 214, CB 216, CB 217, and CB 232. The images were centered at the positions of the YSO candidates listed in Table 1. The NICMOS 3 array had 256×256 pixels, and was used at a plate scale of 0.9 arcsec/pixel, resulting in a field of view of 3.8×3.8 arcmin^2 in the sky. For each globule, we obtained a set of 3×3 dithered frames. Each frame overlapped the previous by 2 arcmin, resulting in a total covered area of about 7.5×7.5 arcmin^2. The integration time per frame was 120 s at J, and 60 s at H and at K.

By median filtering across each set of nine dithered images, stars were removed and a sky frame was obtained. This sky frame was subtracted from each of the nine data images. Dome flats were then used to flatfield the data images (except for the H band where no dome flat was available. The H-band images were flatfielded using the sky frames). The final flatfielded images were subsequently corrected for the presence of bad pixels and mosaicked, coadding the overlapping regions. We restricted our attention to these overlapping regions which formed a central area of about 4.′5×4.′5, which had reduced background noise level σ compared to the remaining area. The values of σ were about 21.5 mag arcsec^{-2} in the J-band images, 20.5 mag arcsec^{-2} in the H-band images, and 20 mag arcsec^{-2} in the K-band images.

2.2 SQIID Data

Nineteen globules (CB 3, CB 6, CB 28, CB 30, CB 31, CB 32, CB 34, CB 35, CB 39, CB 50, CB 52, CB 54, CB 55, CB 60, CB 230, CB 240, CB 244, CB 247, and CB 248) were observed during 1991 November 23–25, using the Kitt Peak National Observatory 1.3 m telescope equipped with the 256×256 pixel SQIID camera. We obtained 18 dithered images (two sets of 3×3 images) of each globule (shifted by 20″–40″ from one another). The integration time per frame was 120 s in each of the J, H, and K bands. The plate scale used was 1.3 arcsec/pixel, resulting in a total coverage of about 6×6 arcmin^2. The images were reduced following similar steps as described for the NICMOS 3 data. We restricted our attention to the overlapping regions which formed a central area of about 5′×5′, which had reduced background noise level σ compared to the remaining area. The values of σ were about 21 mag arcsec^{-2} in the J-band images, 20 mag arcsec^{-2} in the H-band images, and 20 mag arcsec^{-2} in the K-band images.

3. RESULTS

3.1 Search For Nebular Emission

The resulting images were examined for evidence of embedded YSOs in the form of nebulosity associated with a stellar object. If no nebulosity was present in the images, a search for very "red" stellar objects was performed, that is, stellar objects that could be visually estimated to be much brighter in the K-band images than in the corresponding J-band images.

Table 1 lists the results of this image inspection. In the table, column (1) identifies the YSO candidates (Yun 1992). Columns (2) and (3) give the coordinates of the center of the frames (these are also the coordinates of the *IRAS* point sources found in the *IRAS* coadded images; Yun & Clemens 1990). Column (4) indicates the detector used to obtain the images. Column (5) indicates whether there was nebulosity in the corresponding near-infrared images. Column (6) indicates if a red object was present on the images. A near-infrared counterpart was inferred, according to the above criteria, if either column (5), or column (6), or both columns, contained a "Yes." Column (7) indicates the presence of

TABLE 1. Near-infrared survey of YSO candidates in Bok globules: Source coordinates and visual examination properties.

YSO candidate	R. A. (1950)	Decl. (1950)	Detector	Extended nebulosity	Red object	Stellar multiplicity	Spectral Index (12/25 μm)
(1)	(2)	(3)	(4)	(5)	(6)	(7)	(8)
CB3YC1	$0^h26^m04^s$	56°26′05″	SQIID	Yes	Yes	No	0.90
CB6YC1	$0^h46^m25^s$	50°28′36″	SQIID	Yes	Yes	No	−1.43
CB28YC1	$5^h03^m48^s$	−4°02′24″	SQIID	No	No	No	1.33
CB30YC1	$5^h27^m06^s$	5°44′38″	SQIID	No	No	No	0.18
CB31YC1	$5^h30^m47^s$	−0°38′15″	SQIID	Yes	Yes	No	0.65
CB32YC1	$5^h33^m53^s$	−0°19′27″	SQIID	Yes	Yes	No	0.50
CB34YC1	$5^h44^m02^s$	20°59′36″	SQIID	No	Yes	No	−0.67
CB35YC1	$5^h44^m31^s$	10°23′55″	SQIID	No	No	No	1.14
CB39YC1	$5^h59^m05^s$	16°30′47″	SQIID	No	Yes	No	−0.17
CB50YC1	$6^h31^m28^s$	7°51′16″	SQIID	No	No	No	1.41
CB52YC1	$6^h46^m23^s$	−16°50′30″	SQIID	Yes	Yes	Yes	0.76
CB54YC1	$7^h01^m58^s$	−16°18′19″	SQIID	Yes	Yes	Yes	−0.37
CB55YC1	$7^h02^m35^s$	−16°32′38″	SQIID	No	No	No	2.51
CB60YC1	$8^h2^m38^s$	−31°21′37″	SQIID	Yes	Yes	Yes	0.70
CB81YC1	$17^h19^m19^s$	−27°05′20″	NICMOS	No	No	No	−1.50
CB87YC1	$17^h21^m48^s$	−24°09′06″	NICMOS	No	No	No	0.15
CB90YC1	$17^h35^m33^s$	−19°42′57″	NICMOS	No	No	No	0.30
CB128YC1	$18^h13^m17^s$	−3°50′44″	NICMOS	No	Yes	No	1.81
CB142YC1	$18^h27^m10^s$	−13°42′51″	NICMOS	No	Yes	No	1.14
CB171YC1	$18^h59^m12^s$	−4°38′17″	NICMOS	No	No	No	0.50
CB180YC1	$19^h03^m35^s$	−6°56′38″	NICMOS	No	No	No	1.21
CB188YC1	$19^h17^m57^s$	11°30′18″	NICMOS	Yes	Yes	No	−0.51
CB203YC1	$19^h41^m42^s$	18°58′27″	NICMOS	No	No	No	0.90
CB205YC1	$19^h43^m22^s$	27°44′01″	NICMOS	Yes	Yes	No	−0.84
CB206YC1	$19^h44^m23^s$	18°57′49″	NICMOS	No	No	No	−0.18
CB214YC1	$20^h01^m54^s$	26°29′42″	NICMOS	No	Yes	No	−1.88
CB216YC1	$20^h03^m45^s$	23°18′25″	NICMOS	Yes	Yes	No	−0.52
CB217YC1	$20^h05^m55^s$	36°58′14″	NICMOS	No	No	No	0.65
CB230YC1	$21^h16^m58^s$	68°03′22″	SQIID	Yes	Yes	Yes	−0.29
CB232YC1	$21^h35^m09^s$	43°06′32″	NICMOS	No	Yes	No	−0.33
CB240YC1	$22^h31^m49^s$	58°16′37″	SQIID	No	Yes	No	−0.04
CB244YC1	$23^h23^m42^s$	73°57′31″	SQIID	No	Yes	No	−0.71
CB247YC1	$23^h54^m58^s$	64°30′21″	SQIID	No	No	No	−0.74
CB248YC1	$23^h59^m17^s$	47°53′33″	SQIID	No	No	No	0.87
Fraction				0.32	0.58	0.12	

resolved binaries or multiple stars embedded in a common nebulosity. In column (8), we present the values of the *IRAS*-based spectral indices ($\alpha \equiv [d \log(\nu S_\nu)]/[d \log \nu]$, Adams *et al.* 1987; Yun & Clemens 1990), between the wavelengths of 12 and 25 μm for the *IRAS* point sources.

We found that 20 globule images showed evidence for embedded YSOs. Eleven of these images showed objects with near-infrared nebulosity. Of these 11 objects, four display evidence of a binary companion and common nebulosity. The objects found were generally located at the centers of the images, corresponding to the positions of the *IRAS* point source YSO candidates listed in Table 1. A small fraction (~10%) of the near-infrared objects were not located at the center of the images, but were within 90″ of these positions.

In the next section, we analyze the properties of the 11 YSOs displaying extended nebulosity in at least one of their near-infrared images, J, H, or K.

3.2 YSOs Exhibiting Extended Nebular Emission

In this section, we present isophotes of the near-infrared images of the 11 globules showing nebular emission (a "Yes" in column 4 of Table 1). For each globule, a map of the full central area of the image is presented [Figs. 1(a)–14(a)], together with an enlarged map of the portion of the image containing the relevant object and the associated nebulosity as well as some unrelated comparison stars [Figs. 1(b)–14(b)]. The first contour is at the 3σ level, where σ represents the sky background noise in each image. Values of σ are given in the corresponding figure captions.

3.2.1 CB3

Figure 1(a) shows the near-infrared J-band image of CB3. It covers an area of about 5′×5′ towards the first YSO candidate in the CB3 cloud, CB3YC1 (IRAS 00259+5625). Figure 1(b) is a 4.5 times enlargement of the central area of Fig. 1(a). The bright central object (B) shown in Fig. 1(b) is surrounded by tenuous nebulosity and is likely to be the near-infrared counterpart of CB3YC1. The nebulosity has a very limited angular extent, lending a fuzzy appearance to the star image. This object (B) appears on the optical wavelength Palomar prints as a very faint stellarlike source and, unlike the two stars to the north (C) and to the south (D), source B is a very red object. Both a molecular outflow (Yun & Clemens 1992) and a water maser (Scappini *et al.* 1991) have been found in association with the *IRAS* PSC source. The molecular outflow exhibits two wide overlapping lobes with no obvious morphological similarity to the extended near-infrared nebulosity (Yun & Clemens 1994a). The H and K band images appear similar to the J image.

3.2.2 CB6

Figures 2(a), 3(a), and 4(a) show the near-infrared J, H, and K images of CB6. They cover an area of about 5′×5′ toward the YSO-candidate CB6YC1 (IRAS 00465+5028). Figures 2(b), 3(b), and 4(b) are 4.5-times enlargements of the central areas of Figs. 2(a), 3(a), and 4(a), respectively. A crescent-shaped nebulosity (source B) marks the center of

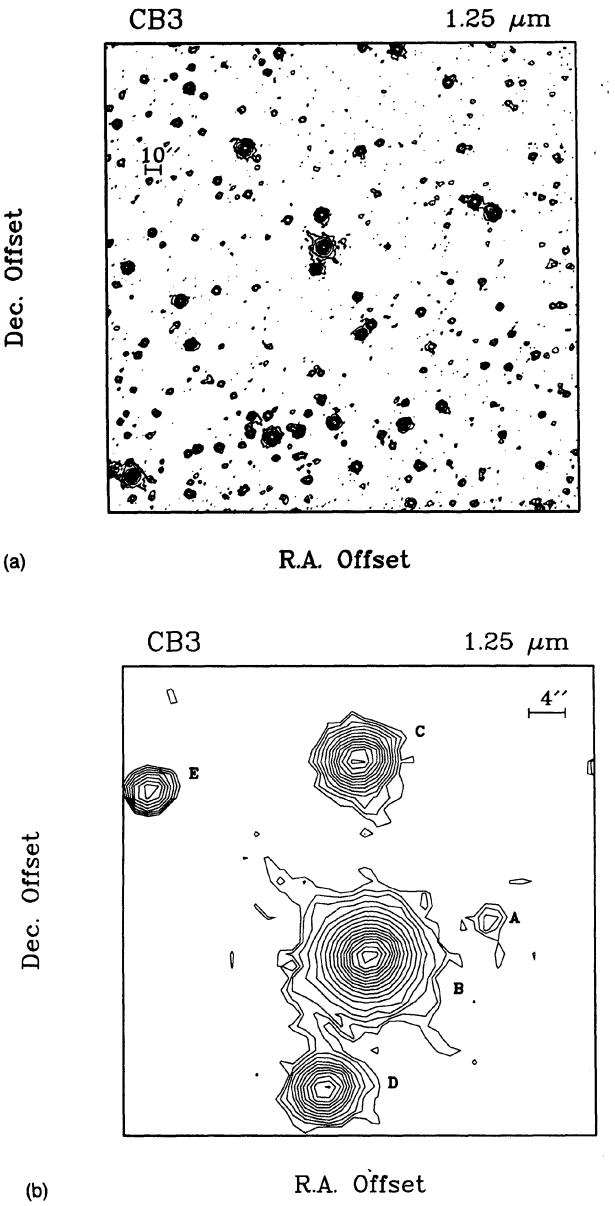

FIG. 1. (a) Isophotes of the near-infrared image (J band) of CB3 covering an area of about 5′×5′ towards CB3YC1. The first contour line corresponds to a surface brightness of 21.2 mag arcsec^{-2}. The contour lines are stepped by 1.2 mag arcsec^{-2}. (b) Isophotes of the central region of CB3 showing the near-infrared nebulosity (J band) associated with the YSO-candidate near-infrared counterpart (object B) in CB3. Very faint nebulosity is seen in the H and K images. The first contour line corresponds to a surface brightness of 21.2 mag arcsec^{-2}. The contour lines are stepped by 0.5 mag arcsec^{-2}.

these images. The B source in the J-band image does not exhibit any well-defined, starlike peak. The B source in the H-band image exhibits a broad peak near the southern end of the crescent, with a full width at half-maximum (FWHM) of 7″. In the K-band image, the B source has a better-defined, narrower peak (FWHM=4″). The FWHM of unrelated stars in the K-band image is about 3″. From a comparison of the three images, we can see that there is a color gradient present, with the western part of the nebula being redder than the eastern part. The nebula has an angular extent of about

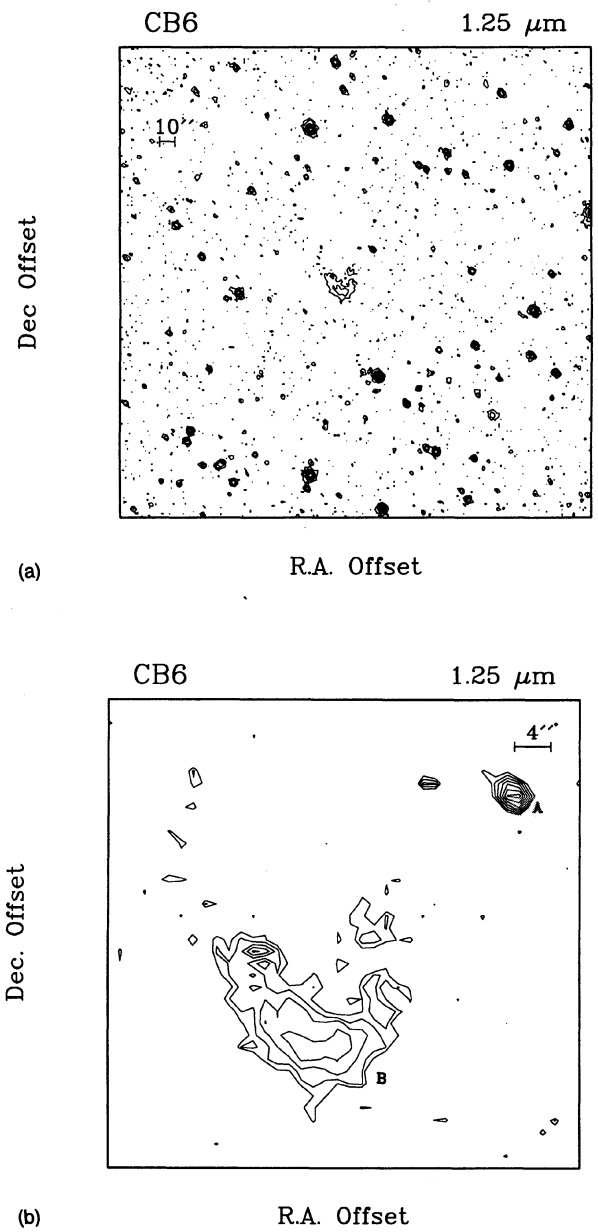

FIG. 2. (a) Isophotes of the near-infrared image (J band) of CB6 covering an area of about 5′×5′ towards CB6YC1. The first contour line corresponds to a surface brightness of 21.2 mag arcsec^{-2}. The contour lines are stepped by 1.2 mag arcsec^{-2}. (b) Isophotes of the central region of CB6 showing the near-infrared nebulosity (J band) associated with the YSO-candidate near-infrared counterpart (object B) in CB6. Source A to the NW is a red object not present on the Palomar prints. The first contour line corresponds to a surface brightness of 21.2 mag arcsec^{-2}. The contour lines are stepped by 0.5 mag arcsec^{-2}.

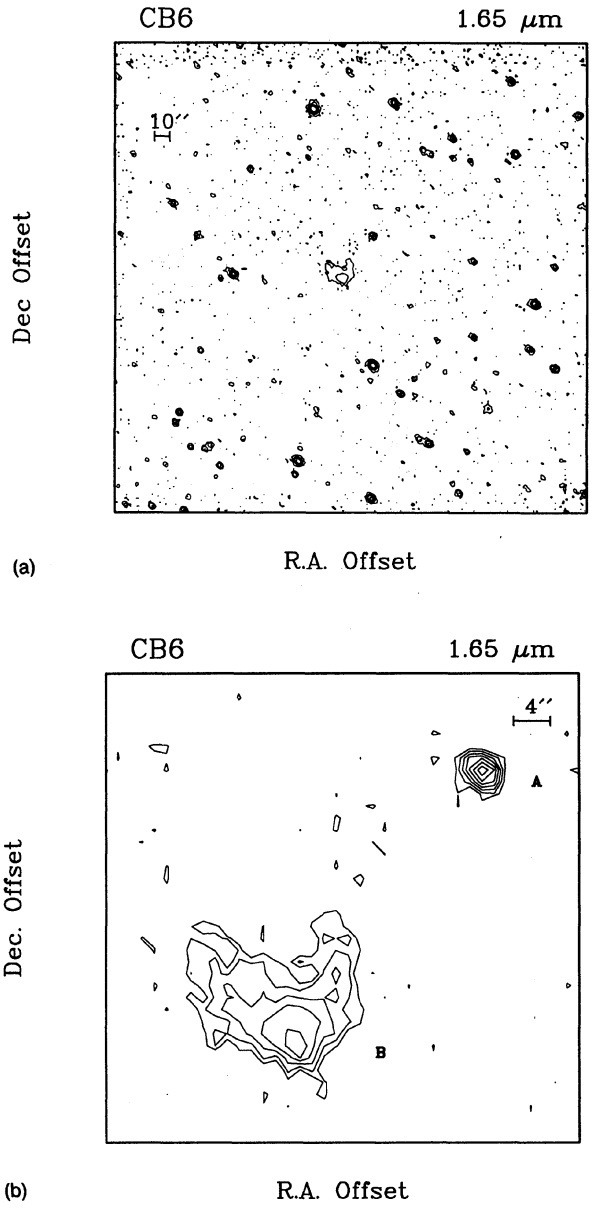

FIG. 3. (a) Isophotes of the near-infrared image (H band) of CB6 covering an area of about 5′×5′ towards CB6YC1. The first contour line corresponds to a surface brightness of 19.6 mag arcsec^{-2}. The contour lines are stepped by 1.2 mag arcsec^{-2}. (b) The same as Fig. 4.2(a) but for the H band. The first contour line corresponds to a surface brightness of 19.6 mag arcsec^{-2}. The contour lines are stepped by 0.5 mag arcsec^{-2}.

12″ which, at a mean distance of 600 pc (Clemens & Barvainis 1988), corresponds to about 7000 AU.

From this set of images, we are unable to conclude whether the nebulosity seen lodges an embedded star. The morphology of the nebulosity is reminiscent of a bow shock. For example, the similarity of the shape of source CB6-B to the shape of Herbig–Haro object HH34, studied by Burhke & Mundt (1986), and Reipurth & Graham (1988), is striking. This could be an indication of the presence of shock excited gas (e.g., Reipurth 1991) with no embedded star in this nebula. Alternatively, the progressively better-defined stellar-like peaks, from the J image towards the longer-wavelength K image, resemble those seen in the JHK images of the CG30 (HH120) and SA111 (HH46) clouds (both known to lodge embedded stars) obtained by Graham (1988). He attributed the nebulosity seen at J and H to scattered light from an embedded star whose image becomes less extincted and more sharply defined at K.

Source A to the NW, about 50″ away from the peak seen in the K-band image, is a very red object not present on the Palomar prints.

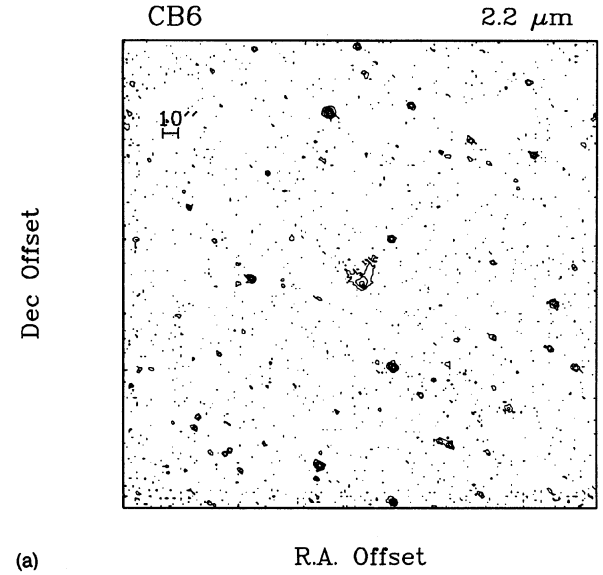

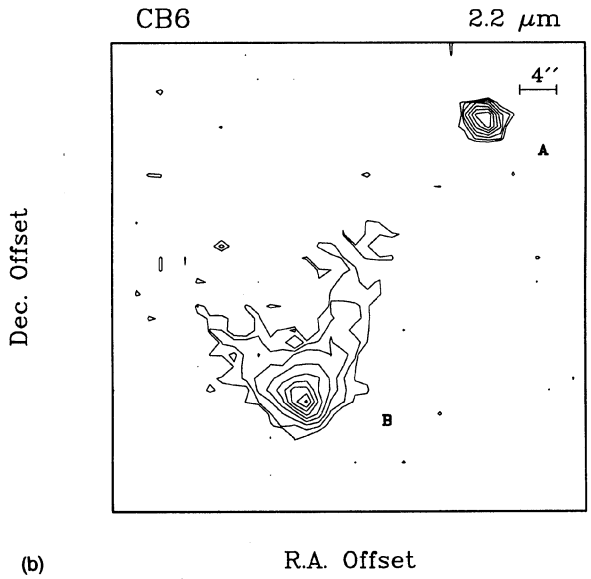

FIG. 4. (a) Isophotes of the near-infrared image (K band) of CB6 covering an area of about 5′×5′ towards CB6YC1. The first contour line corresponds to a surface brightness of 19.0 mag arcsec^{-2}. The contour lines are stepped by 1.2 mag arcsec^{-2}. (b) The same as (a) but for the K band. The first contour line corresponds to a surface brightness of 19.0 mag arcsec^{-2}. The contour lines are stepped by 0.5 mag arcsec^{-2}.

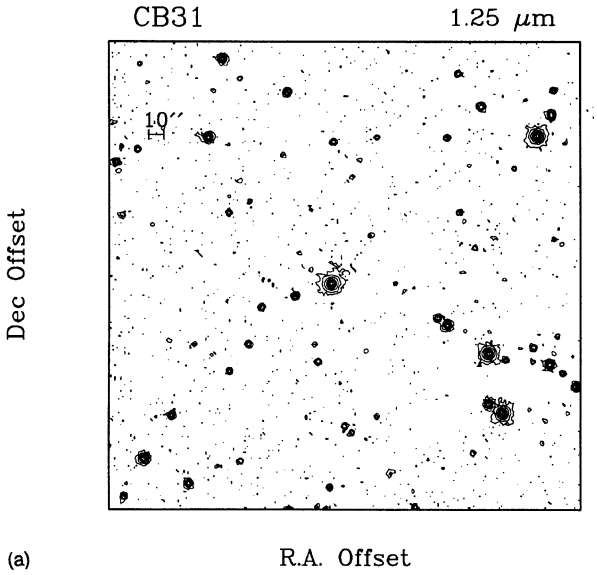

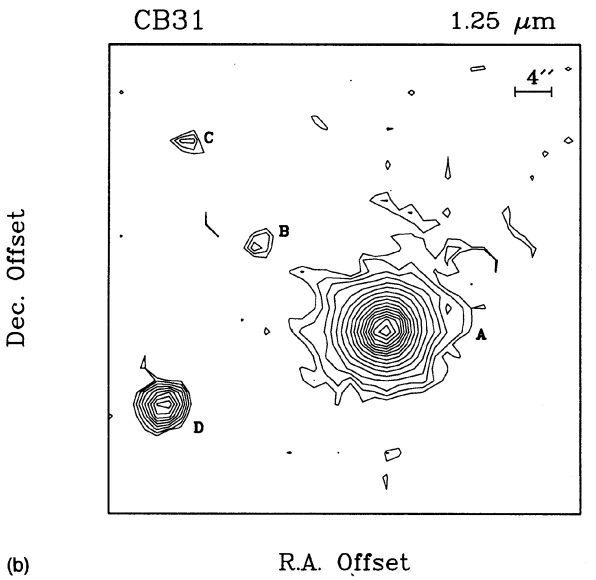

FIG. 5. (a) Isophotes of the near-infrared image (J band) of CB31 covering an area of about 5′×5′ towards CB31YC1. The first contour line corresponds to a surface brightness of 21.2 mag arcsec^{-2}. The contour lines are stepped by 1.2 mag arcsec^{-2}. (b) Isophotes of the central region of CB31 showing the near-infrared nebulosity (J band) associated with the YSO-candidate near-infrared counterpart (object A) in CB31. No nebulosity is seen in the corresponding J and K images. The first contour line corresponds to a surface brightness of 21.2 mag arcsec^{-2}. The contour lines are stepped by 0.5 mag arcsec^{-2}.

CO outflow was not convincingly detected towards CB6 at the levels of our CO outflow search (Yun & Clemens 1992). However, some vestiges of wing emission ($\sim 2\sigma$) were present in the outflow contour map of the red wing integrated CO emission.

3.2.3 CB31

Figure 5(a) shows the near-infrared J-band image of CB31. It covers an area of about 5′×5′ towards the YSO-candidate CB31YC1 (IRAS 05307−0038). Figure 5(b) is a 4.5-times enlargement of the central area of Fig. 5(a). The nebulosity seen around object A is tenuous and faint and has very limited angular extent, lending a fuzzy appearance to the star image. The FWHM of source A is not different from the FWHM of unrelated stars in the image. No extended emission is seen in the H or K images. No outflow has been detected (Yun & Clemens 1992). This object appears on both the O and E Palomar prints and is associated with an optical wavelength reflection nebula.

3.2.4 CB32

Figure 6(a) shows the near-infrared J-band image of CB32. It covers an area of about 5′×5′ towards the YSO-

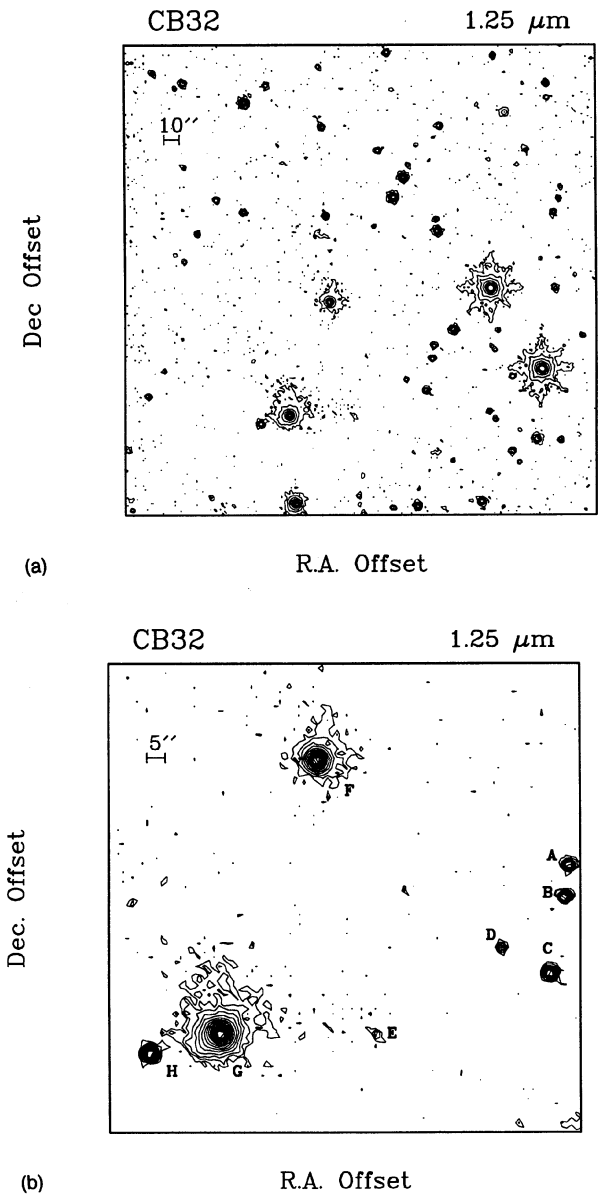

FIG. 6. (a) Isophotes of the near-infrared image (J band) of CB32 covering an area of about $5' \times 5'$ towards CB32YC1. The first contour line corresponds to a surface brightness of 20.7 mag arcsec^{-2}. The contour lines are stepped by 1.2 mag arcsec^{-2}. (b) Isophotes of the central region of CB32 showing the near-infrared nebulosity (J band) associated with the YSO-candidate near-infrared counterpart (objects F or G) in CB32. The nebulosities surrounding these objects extend mostly to the north of the objects. The H-band image is similar but the nebulosity is fainter. No nebulosity is seen in the corresponding K-band image. The first contour line corresponds to a surface brightness of 20.7 mag arcsec^{-2}. The contour lines are stepped by 0.5 mag arcsec^{-2}.

candidate CB32YC1 (IRAS 05337−0019). The diffuse appearance of the two brightest stars to the west is due to diffraction in the telescope and not to nebular emission. Figure 6(b) is a 2-times enlargement of part of Fig. 6(a). There are two bright objects, F and G, surrounded by nebular emission. In both objects, the nebulosities are not spherically distributed around the objects nor distributed like the diffraction spikes of the two brightest stars [see Fig. 6(a)], but instead extend mostly towards the north in a cometary or jetlike fashion. The two objects are well separated (1.5 arcmin or 0.26 pc at 600 pc distance) and the respective nebulosities do not overlap. Thus, the two objects are likely not to form a binary system. The nebulosity around each object is bluer in the infrared bands than the object and is likely due to scattered light from the objects. Inspection of the Palomar plates shows that the northern object, F, is at the center of an optical nebula, possibly a reflection nebula. The southern object, G, is at the edge of an area of optical nebulosity.

Both in this case and in CB31, what we see in the J-band image is close to what is seen in the optical photographs. These YSOs may have cleared away most of the cloud material surrounding their birth places and may be illuminating the remaining cloud material, creating the reflection nebulae seen both in the optical and in the "bluest" of the near-infrared bands (J band). In addition, we note that, for both CB31YC1 and CB32YC1, their 12/25 μm spectral indices are positive and similar (0.65 and 0.50), and we found no CO outflow to be associated with either of these YSO candidates.

3.2.5 CB52

Figure 7(a) shows the near-infrared J-band image of CB52. It covers an area of about $5' \times 5'$ towards the YSO-candidate CB52YC1 (*IRAS* 06464−1650). Figure 7(b) is a 3.5-times enlargement of the central area of Fig. 7(a). At the center of Fig. 7(b), we found two starlike objects, C and D, embedded in common nebulosity. Both objects can be seen in the H- and K-band images but no nebulosity is present in either band. The two objects are separated by 9″ with the fainter one being redder and not present on the Palomar prints, while the brighter one is somewhat bluer and visible on both the O and the E POSS prints.

3.2.6 CB54

Figure 8(a) shows the near-infrared K-band image of CB54. It covers an area of about $5' \times 5'$ towards the YSO-candidate CB54YC1 (IRAS 07020−1618). Figure 8(b) is a 2.5-times enlargement of the central area of Fig. 8(a). CB54 seems to be lodging several red or nebulous objects. Of all the objects seen in the K-band image [Fig. 8(b)] only objects D, E, H, J, and K appear on the Palomar prints. Because of their relatively blue colors, these objects are likely to be foreground field stars unrelated to the cloud. Objects A, C, F, and L appear as extremely faint objects or are not present in the J-band image. Object B is a much fainter object in the J-band image.

The axis of the bipolar outflow found in CB54 (Yun & Clemens 1992; Yun *et al.* 1993) is directed along the NE–SW direction and is roughly perpendicular to the line connecting objects C and F, which are by far the reddest objects in the field. These two objects are separated by 12″ (7000 AU at 600 pc). They are contained within common nebulosity and could possibly constitute an embedded binary stellar system.

The nebulous emission is virtually absent in the J band whereas it is extremely bright in the K band. If the nebulos-

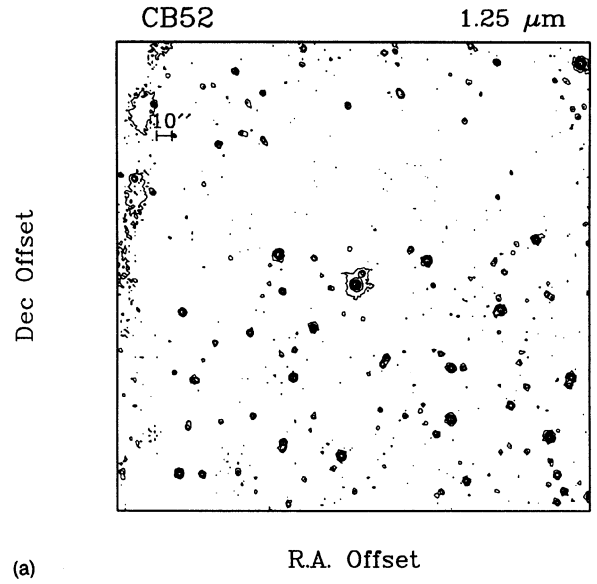

FIG. 7. (a) Isophotes of the near-infrared image (J band) of CB52 covering an area of about $5'\times5'$ towards CB52YC1. The first contour line corresponds to a surface brightness of 20.7 mag arcsec^{-2}. The contour lines are stepped by 1.2 mag arcsec^{-2}. (b) Isophotes of the central region of CB52 showing the near-infrared nebulosity (J band) associated with the YSO-candidate near-infrared counterpart (the pair of objects C and D) in CB52. These two central objects can be seen in the H and K images but no nebulosity is present in these images. The first contour line corresponds to a surface brightness of 20.7 mag arcsec^{-2}. The contour lines are stepped by 0.5 mag arcsec^{-2}.

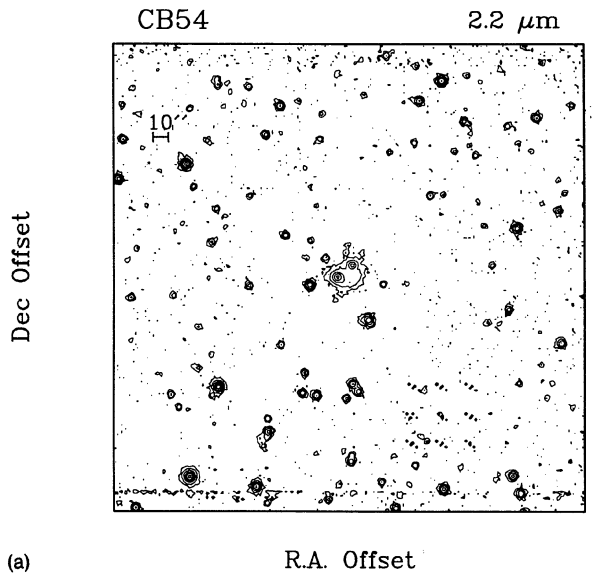

FIG. 8. (a) Isophotes of the near-infrared image (K band) of CB54 covering an area of about $5'\times5'$ towards CB54YC1. The first contour line corresponds to a surface brightness of 19.0 mag arcsec^{-2}. The contour lines are stepped by 1.2 mag arcsec^{-2}. (b) Isophotes of the central region of CB54 showing the near-infrared nebulosity (K band) associated with the YSO-candidate near-infrared counterpart (the pair of objects C and F) in CB54. Several objects may be embedded in the cloud. Only objects D, E, H, J, and K are visible stars. Very little nebulosity is seen in the corresponding J-band image. Faint nebulosity is seen in the H-band image. The first contour line corresponds to a surface brightness of 19.0 mag arcsec^{-2}. The contour lines are stepped by 0.5 mag arcsec^{-2}.

ity seen is due to scattered stellar light, then either all the shorter wavelength emission (e.g., J band) is extincted before escaping the cloud, or the spectrum of the illuminator is exceedingly red, with very little light emitted shortwards of $\sim$1–2 μm. In either case, the illuminator(s) are likely to be very embedded and young, probably the youngest YSOs found in this survey.

3.2.7 CB60

Figure 9(a) shows the near-infrared J-band image of CB60. It covers an area of about $5'\times5'$ towards the YSO-candidate CB60YC1 (IRAS 08026−3122). Figure 9(b) is a 3.5-times enlargement of the central area of Fig. 9(a). The brightest object in Fig. 9(b) (object D), is present on the Palomar prints surrounded by nebulosity. However, the

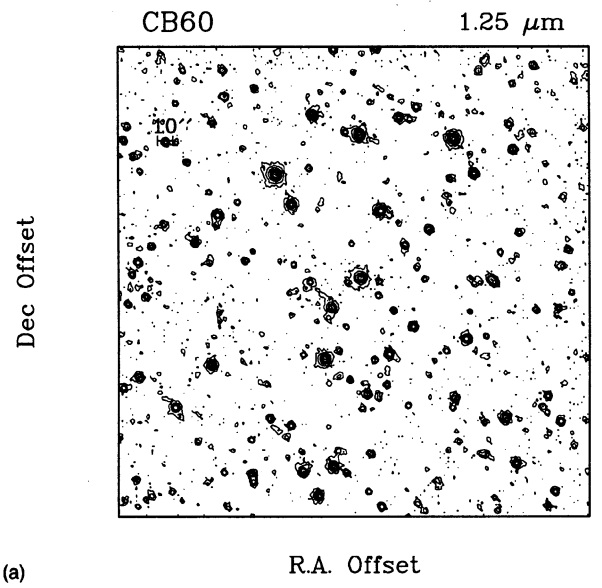

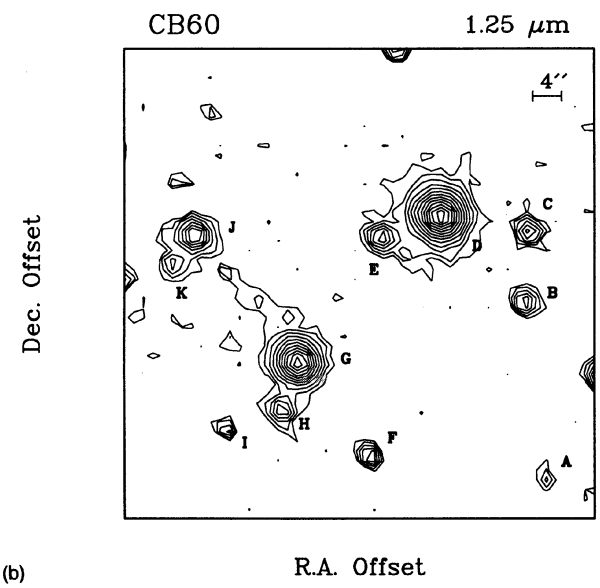

FIG. 9. (a) Isophotes of the near-infrared image (J band) of CB60 covering an area of about 5′×5′ towards CB60YC1. The first contour line corresponds to a surface brightness of 20.7 mag arcsec^{-2}. The contour lines are stepped by 1.2 mag arcsec^{-2}. (b) Isophotes of the central region of CB60 showing the near-infrared nebulosity (J band) associated with the YSO-candidate near-infrared counterpart (the pair of objects D and E) in CB60. The fainter central object (E) does not show on the Palomar prints and may be a binary companion. No nebulosity is seen in the corresponding H and K images. The first contour line corresponds to a surface brightness of 20.7 mag arcsec^{-2}. The contour lines are stepped by 0.5 mag arcsec^{-2}.

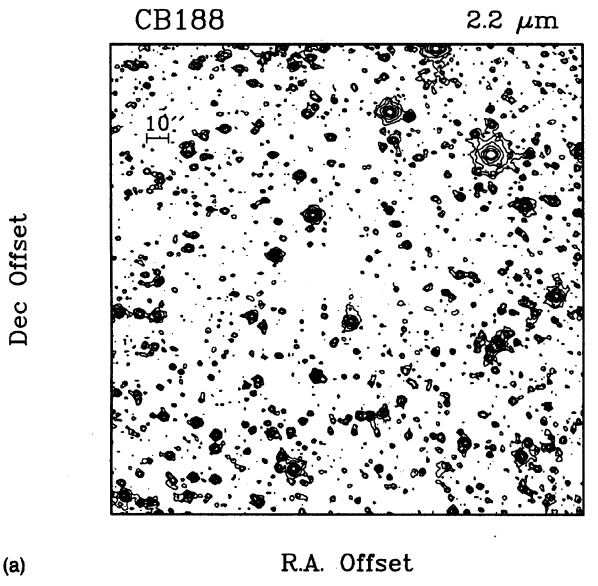

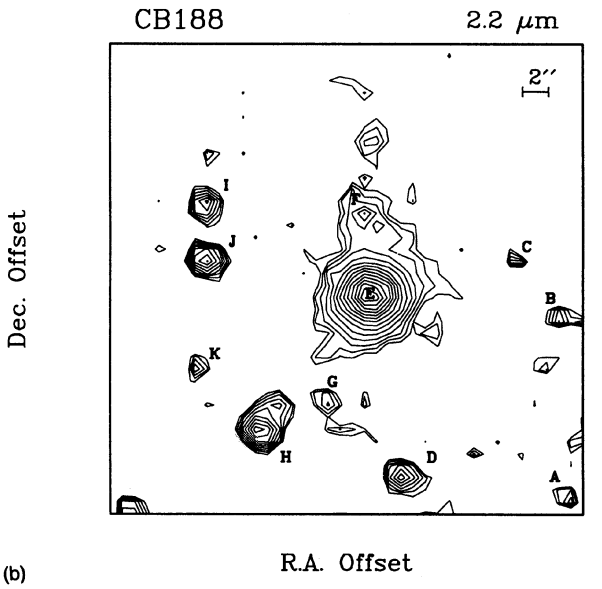

FIG. 10. (a) Isophotes of the near-infrared image (K band) of CB188 covering an area of about 3′.5×3′.5 towards CB188YC1. The first contour line corresponds to a surface brightness of 19.4 mag arcsec^{-2}. The contour lines are stepped by 1.2 mag arcsec^{-2}. (b) Isophotes of the central region of CB188 showing the near-infrared nebulosity (K band) associated with the YSO-candidate near-infrared counterpart (object E) in CB188. No nebulosity is seen in the corresponding J image. Fainter nebulosity is seen in the H-band image. The object shown has no optical counterpart on the Palomar prints. The first contour line corresponds to a surface brightness of 19.4 mag arcsec^{-2}. The contour lines are stepped by 0.5 mag arcsec^{-2}.

fainter companion (E) seen to the east does not appear on the Palomar prints and may be a binary companion. At least two other rather red objects appear in the image, namely objects J and K in Fig. 9(b). The nebulosities seen throughout this image are tenuous and faint.

3.2.8 CB188

Figure 10(a) shows the near-infrared K-band image of CB188. It covers an area of about 3′.5×3′.5 towards the YSO-candidate CB188YC1 (IRAS 19179+1129). Figure 10(b) is a 5-times enlargement of the central area of Fig. 10(b). Object E in this cloud [Fig. 10(b)] has no optical counterpart on the Palomar prints. On those prints and in the J-band image, the location corresponding to object E is near the central area of a very opaque region of the cloud and is well isolated from other stars. In the K-band image, object E is surrounded

by nebulosity with a cometary (or jetlike) morphology (including the F source). Object F may be a binary companion or a bright spot in a stellar jet or outflow cavity extending north of object E (which may also include the faint emission north of F). In the J-band image object E appears as a starlike source and object F is very faint (can barely be distinguished from noise).

In the K-band image other fainter, red sources appear (D, H, I, and J) between about 15 and 60 arcsec away, which may be additional embedded sources or background stars.

3.2.9 CB205/L810

Figure 11(a) shows the near-infrared K-band image of CB205. It covers an area of about 3.'5×3.'5 towards the YSO-candidate CB205YC1 (IRAS 19433+2743). Figure 11(b) is a 3-times enlargement of the central area of Fig. 11(a). The dark cloud CB205 (Lynds 810) displays a very extended infrared nebula [Figs. 11(a) and 11(b)] and an extended optical reflection nebula on the POSS. A wealth of interesting phenomena was observed to be associated with this cloud and is described in Yun *et al.* (1993). They found a near-infrared source (L810IRS) at the position where analysis of optical polarization maps (Scarrott *et al.* 1991) predicted the illuminator of the L810 nebula should be located. L810 displays an extended near-infrared nebula which, at the K band, extends symmetrically to the north and the south of L810IRS in a biconical fashion, with good spatial coincidence with the CO outflow lobes. A jetlike feature is also present in the vicinity of the nebula. This feature is particularly prominent at K and points back to L810IRS, indicating that L810IRS is likely to be a very active source.

3.2.10 CB216

Figure 12(a) shows the near-infrared K-band image of CB216. It covers an area of about 3.'5×3.'5 towards the YSO-candidate CB216YC1 (IRAS 20037+2317). Figure 12(b) is a 4-times enlargement of the central area of Fig. 12(a). Object E in this cloud [Fig. 12(b)] exhibits remarkable similarities with object E in CB188 [Fig. 10(b)]. Nebulosities are seen in the K and H bands (but not in J) which exhibit cometary (or jetlike) and fuzzy extensions of the star images. Both in CB188 and CB216, the nebulosities extend to the north of the stars and the extents are comparable. Interestingly, the spectral indices of the YSO candidates are also virtually identical (−0.51 and −0.52, Table 1). In CB216, object E is the "reddest" ($J-K$) stellar object in the field.

The blue lobe of the CO outflow associated with CB216YC1 (Yun & Clemens 1994a) extends to the north, which could be related to the asymmetry in the infrared nebulosity seen if the nebula is due to reflection. If it is due to a stellar jet, it is likely either poorly collimated or bent, because the nebulosity appears resolved in both dimensions. This nebula may be a fainter version of the uniconical nebula seen in CB230, below.

3.2.11 CB230

Figures 13(a) and 14(a) show the near-infrared J and K images of CB230. They cover an area of about 5′×5′ towards the YSO-candidate CB230YC1 (IRAS 21169+6804). Figures 13(b) and 14(b) are 4-times enlargements of the central areas of Figs. 13(a) and 14(a), respectively. Two objects (A and B) appear at the center of these images. They are surrounded by nebular emission and isolated from any other

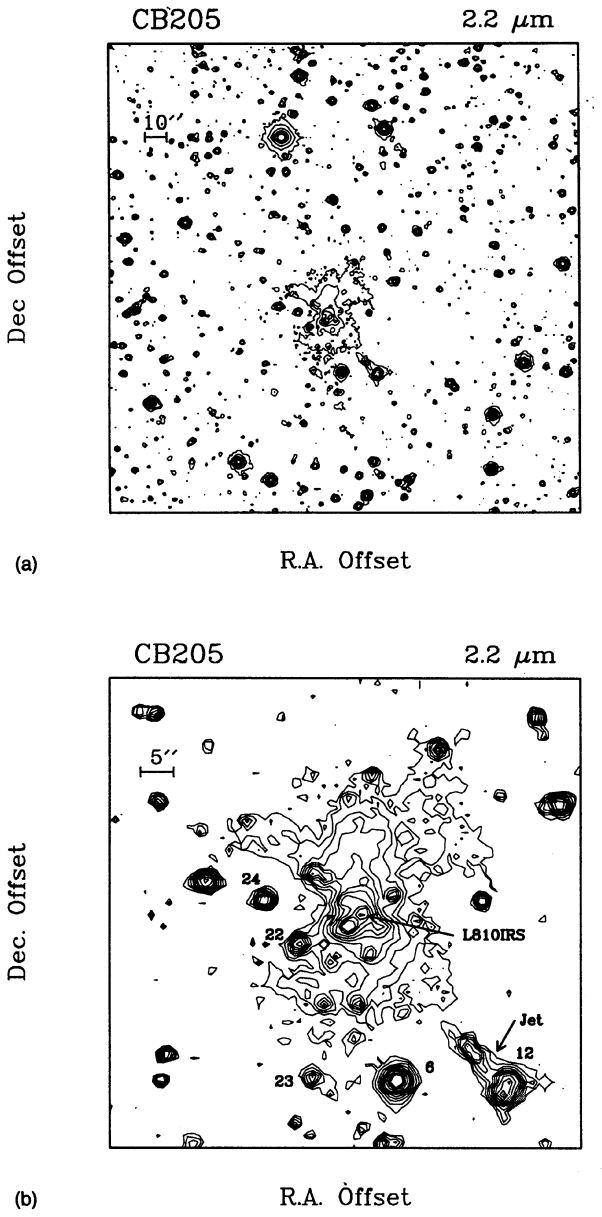

FIG. 11. (a) Isophotes of the near-infrared image (K band) of CB205/L810 covering an area of about 3.'5×3.'5 towards CB205YC1. The first contour line corresponds to a surface brightness of 18.7 mag arcsec^{-2}. The contour lines are stepped by 1.2 mag arcsec^{-2}. (b) Isophotes of the central region of CB205/L810 showing the near-infrared nebulosity (K band) associated with the YSO-candidate near-infrared counterpart in CB205. Notice the extended nebula and its symmetric, hourglass shape in this K-band image. In the corresponding J-band image the northern part of the nebula is absent. The star numbers indicated in this figure are according to the nomenclature of Neckel & Staude (1990). The first contour line corresponds to a surface brightness of 18.7 mag arcsec^{-2}. The contour lines are stepped by 0.5 mag arcsec^{-2}.

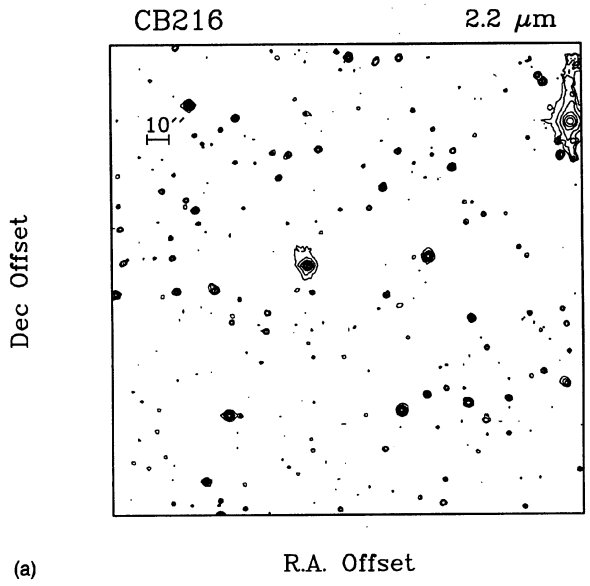

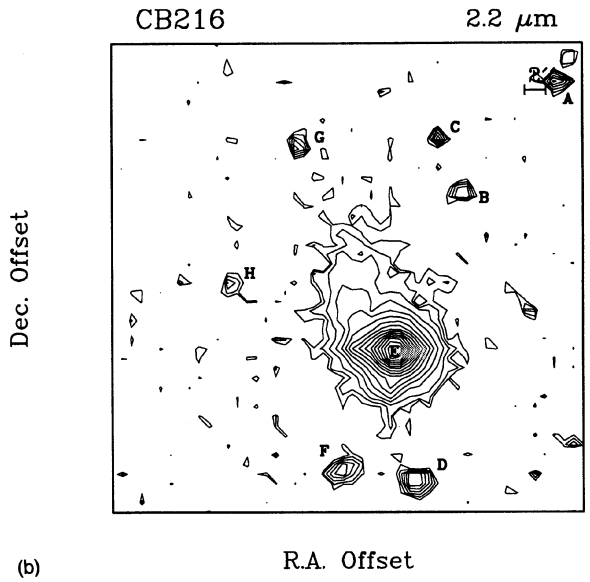

FIG. 12. (a) Isophotes of the near-infrared image (K band) of CB216 covering an area of about 3′.5×3′.5 towards CB216YC1. The first contour line corresponds to a surface brightness of 19.4 mag arcsec^{-2}. The contour lines are stepped by 1.2 mag arcsec^{-2}. (b) Isophotes of the central region of CB216 showing the near-infrared nebulosity (K band) associated with the YSO-candidate near-infrared counterpart (object E) in CB216. No nebulosity is seen in the corresponding J image. Fainter nebulosity is seen in the H-band image. The morphology of the extended emission is similar to that of the nebula seen toward CB188. The first contour line corresponds to a surface brightness of 19.4 mag arcsec^{-2}. The contour lines are stepped by 0.5 mag arcsec^{-2}.

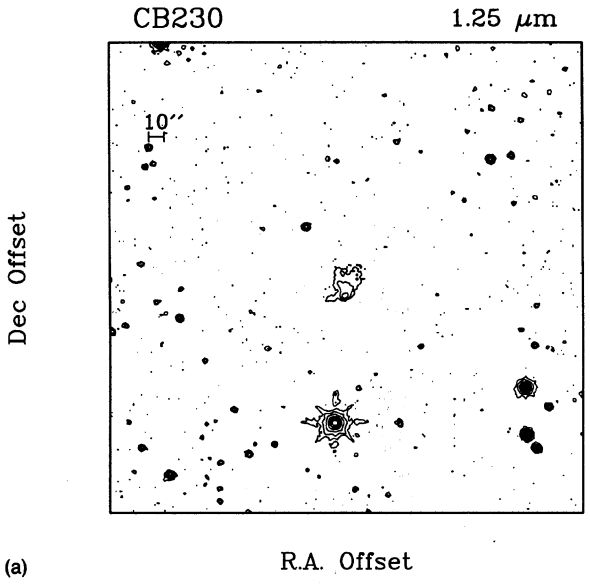

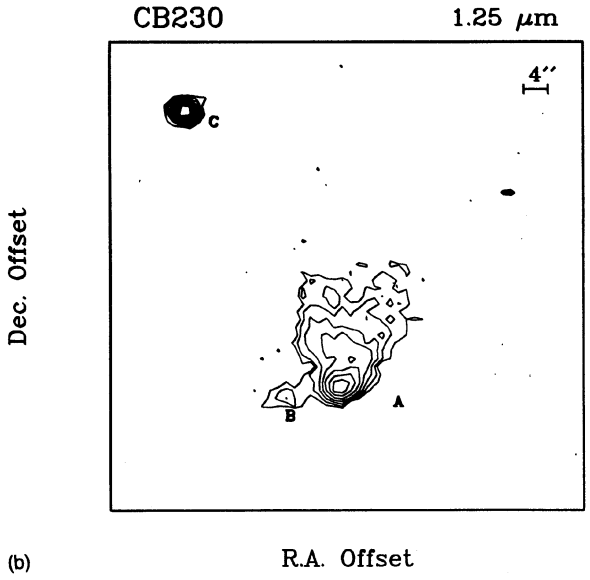

FIG. 13. (a) Isophotes of the near-infrared image (J band) of CB230 covering an area of about 5′×5′ towards CB230YC1. The first contour line corresponds to a surface brightness of 20.7 mag arcsec^{-2}. The contour lines are stepped by 1.2 mag arcsec^{-2}. (b) Isophotes of the central region of CB230 showing the near-infrared nebulosity (J band) associated with the YSO-candidate near-infrared counterpart in CB230. The first contour line corresponds to a surface brightness of 20.7 mag arcsec^{-2}. The contour lines are stepped by 0.5 mag arcsec^{-2}.

star in the field. The separation between the objects is 12″ (about 7000 AU at 600 pc distance), hence these objects may represent an embedded binary system.

The nebulosity is conspicuous in all near-infrared bands, but is more extended and brighter in K. No star or nebulosity is seen on the Palomar prints.

In the J-band image, object B is very faint. Object A has a more diffuse appearance and is brighter.

The direction of the outflow associated with CB230 is along a north–south axis (Yun & Clemens 1994a), or perpendicular to the line joining the two objects. Given the angular resolution of the CO outflow maps, it is not possible to conclude whether the center of the outflow coincides with one or both of the near-infrared stellar sources. However, most of the near-infrared nebulosity extends towards the north of object A in a uniconical distribution. The blue lobe also extends to the north of the outflow source. If the outflow originates from object A, and if the northern blue lobe has cleared out

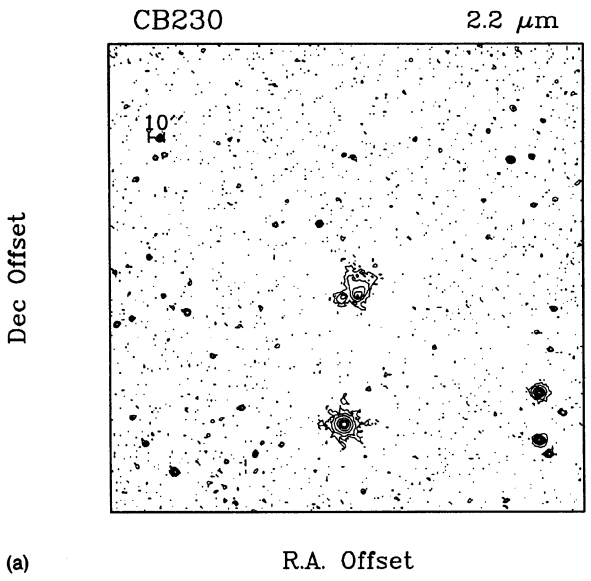

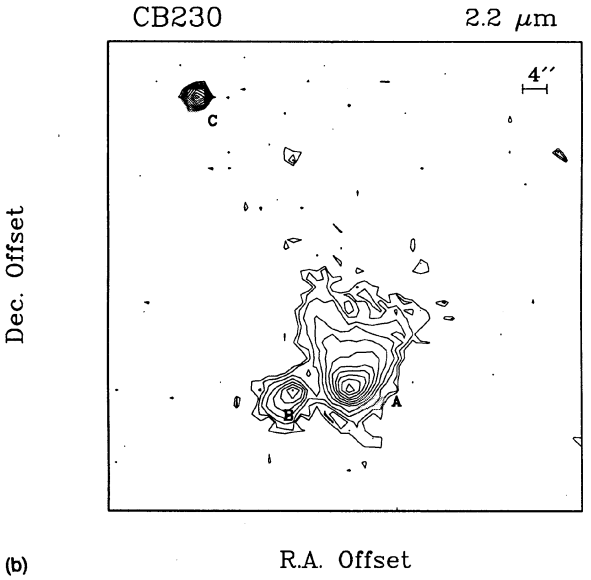

FIG. 14. (a) Isophotes of the near-infrared image (K band) of CB230 covering an area of about 5′×5′ towards CB230YC1. The first contour line corresponds to a surface brightness of 19.0 mag arcsec^{-2}. The contour lines are stepped by 1.2 mag arcsec^{-2}. (b) Isophotes of the central region of CB230 showing the near-infrared nebulosity (K band) associated with the YSO-candidate near-infrared counterpart in CB230. The two objects involved in the nebulosity may constitute a binary system. The first contour line corresponds to a surface brightness of 19.0 mag arcsec^{-2}. The contour lines are stepped by 0.5 mag arcsec^{-2}.

cloud material from the front edge of the cloud, it may have formed a cavity. Scattered light from the walls of this cavity could result in the more extended northern emission relative to the southern part of the nebula (as for L810; Yun *et al.* 1993). In the K-band image, object B is elongated to the SE of that source.

3.3. Tabulation of Results

In Table 1, we presented the general results of the visual inspection for all the YSO-candidates surveyed. Tables 2–4 summarize most of the information regarding the visual inspection of the YSO-candidate images, for objects exhibiting extended nebular emission. Photometry of the stellar sources is contained in the fourth paper in this series (Yun & Clemens 1994b).

Table 2 shows a breakdown of the 34 globules surveyed: our visual examination identified 20 stellar objects that were much brighter at K than at J. Of these 20 objects, 11 appear associated with nebulosity.

In Table 3, column (1) identifies the YSO candidates. Col-

TABLE 2. Near-infrared survey of YSOs in Bok Globules: YSO candidates with extended nebulosity.

YSO candidate	Near-infrared band	Stellar multiplicity	Spectral Index (12/25 μm)	Palomar nebulosity	Outflow detected
(1)	(2)	(3)	(4)	(5)	(6)
CB3YC1	J,H,K	No	0.90	No	Yes
CB6YC1	K,H,J	No	−1.43	No	No
CB31YC1	J	No	0.65	O,E	No
CB32YC1	J,H	No	0.50	O,E	No
CB52YC1	J	Yes	0.76	O,E	No
CB54YC1	K,H	Yes	−0.37	No	Yes
CB60YC1	J	Yes	0.70	O,E	...[a]
CB188YC1	K,H	No	−0.51	No	Yes
CB205YC1	K,H,J	No	−0.84	E,O	Yes
CB216YC1	K,H	No	−0.52	No	Yes
CB230YC1	K,H,J	Yes	−0.29	No	Yes

Note to TABLE 2

[a]Not searched for molecular outflow.

TABLE 3. YSO candidates with extended nebulosity: Properties of the nebulosity.

YSO candidate	Nebula extent	Nebula shape	Nebula orientation	Peak Nebula surface brightness[a]
	(″)		(°)	(mag arcsec^{-2})
CB3YC1	6	fuzzy	...	13.2
CB6YC1	12	cometary	0	15.0
CB31YC1	6	fuzzy	...	13.2
CB32YC1	12	cometary	0	13.4 14.0
CB52YC1	6	fuzzy	−30[b]	14.2 17.7
CB54YC1	8	bipolar	−40[b]	14.0 15.0
CB60YC1	6	fuzzy	...	14.7 18.2
CB188YC1	12	cometary	0	12.5
CB205YC1	20	bipolar	0	13.4
CB216YC1	12	cometary	30	11.9
CB230YC1	16	cometary	0	14.0

Notes to TABLE 3

[a]For the band indicated first in column (2) of Table 2. Two values are given when two objects are contained in the nebulosities.

[b]Position angle of the stellar axis of the binary.

TABLE 4. YSO candidates with extended nebulosity: Classification of the nebulosity.

YSO candidate	Nebula extent (″)	Nebula shape			
		Primary shape	Brightness	Secondary shape	Brightness
CB3YC1	6	fuzzy	F	...	...
CB6YC1	12	crescent (uniconical?)	B	...	...
CB31YC1	6	fuzzy	F	...	...
CB32YC1	12	fuzzy	F	colinear segment	F
CB52YC1	6	common, elliptical	B	...	...
CB54YC1	8	common, elliptical	B	arc	B
CB60YC1 DE[a]:	6	common	F	...	...
CB60YC1 GH[b]:	6	common	F	arc	F
CB188YC1	12	colinear lobe	B	...	...
CB205YC1	20	biconical	B	colinear segment	B
CB216YC1	12	arc	B	...	...
CB230YC1	16	uniconical	B	common	B

Notes to TABLE 4

[a]Nebulosity involving objects D and E in Fig. 9(b).
[b]Nebulosity involving objects G and H in Fig. 9(b).

umn (2) indicates the band in which nebulosity is seen. More than one letter in that column indicates that the nebulosity is seen in several bands (J,H,K) but is brighter or more extended in the band indicated first. Columns (3) and (4) are as in Table 1. The presence of nebulosity and the relative color of the nebula in the Palomar prints ("O" or "E") is indicated in column (5). The detection of a molecular outflow is indicated in column (6) and is taken from Yun & Clemens (1992).

Table 4 summarizes our visual evaluation of the morphologies of the infrared nebulae. Because 5 of the 11 sources appeared to have complex shapes, we have broken the shape classification into two rankings. The primary shape describes the dominant nebular shape, while the secondary shape refers to any underlying departures from the primary descriptor. The brightness columns [(4) and (6)] indicate whether the nebular feature is relatively bright ("B", involving more than just the lowest contours) or relatively faint ("F", involving only the lowest contours).

The shape descriptors were defined as follows: "fuzzy" nebulae appear broader than normal point sources in a mostly axisymmetric fashion, without distinguishing nonaxisymmetric features. "Common, elliptical" means that the nebula envelopes both members of the stellar double, producing isophotes which are roughly elliptical in shape. Features which appear resolved in both dimensions were judged to be either "uniconical" if the nebula was asymmetrically distributed about the star, or "biconical" if the distribution was symmetric. We use the term "conical" to describe the general appearance of these nebulae, which are generally triangle shaped, with one corner, or apex, at the location of the exciting star. Finally there are nebulae which appear mostly resolved in only one dimension, which we refer to as "segments" or "arcs." Features which are mostly linear, and colinear with the stellar core, are listed as "colinear segments." If the feature appears to be an arc segment, or bent, or not colinear with the stellar core, we list it as arc. One source, CB6, has a nonsymmetric shape which has a wider opening angle than the other conical sources. We classify it as "crescent."

In Table 4, the breakdown of primary nebula shapes is as follows: fuzzy (unresolved in 2-dimensions)—3 objects; arcs or colinear segments (resolved in one-dimension)—2 objects; common, elliptical, uniconical, biconical, and crescent (resolved in two dimensions)—6 objects. Of the secondary nebular shapes, four are resolved in one dimension (arcs or segments), and one in two dimensions (common, elliptical type).

This distribution of nebular shapes is similar to the shapes displayed in Tamura *et al.* (1991a) for their 2 μm imaging study of nearby star forming complexes. Of the eight objects they display, six are resolved in both dimensions, one is resolved in only one dimension, and one is unresolved in both dimensions. Tamura *et al.* (1991a) attribute their 2.2 μm nebulosities around young stars to scattering of radiation from the central source by dust associated with mass outflow from a circumstellar dust disk. They did not find evidence of stellar multiplicity, e.g., the presence of resolved binaries or multiple stars, embedded in a common nebulosity.

The information contained in Tables 1–4 is discussed below.

4. DISCUSSION

4.1 The Presence of Near-Infrared Counterparts

We begin by considering the YSO candidates for which *no* nebular or stellar counterpart was detected by visual inspection of the near-infrared images [a "No" in both columns (2) and (3) of Table 1]. Analysis of the 12/25 μm spectral indices shows that, with three exceptions (CB81YC1, CB206YC1, and CB247YC1), this group of 14 YSO candidates is dominated by YSOs whose 12/25 μm spectral indices are positive (mean $\alpha_{12/25}$=0.90; dispersion =0.7).

The spectral indices of the YSO candidates for which the visual inspection has identified a counterpart are distinctively different from the previous nondetection group. In this second group of 20 YSO candidates, more than half exhibit negative 12/25 μm spectral indices. The properties of the two groups are illustrated partially in Fig. 15. Figure 15 shows the cumulative fraction of sources with spectral indices smaller than or equal to a fixed value. The dashed line refers to the group of objects for which the use of our criteria (see Sec. 3) resulted in identifying a near-infrared YSO-candidate; the solid line refers to the group with no YSO counterpart from the visual inspection. Sixty percent of the sources in the former group have negative 12/25 μm spectral

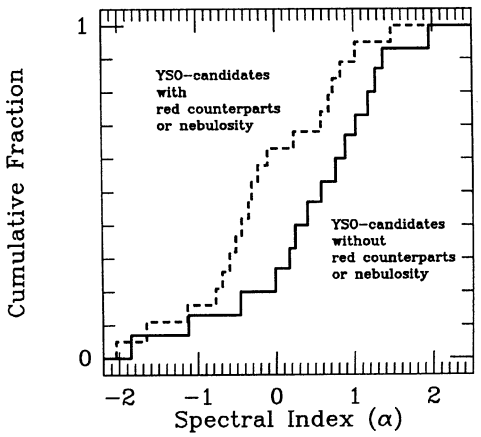

FIG. 15. Cumulative fraction of sources with spectral indices smaller than or equal to a fixed value. The dashed line refers to the group of objects for which our criteria and images provided a counterpart candidate; the dashed line refers to the group with no counterpart candidate from the image inspection. Sixty percent of the sources in the former group have negative 12/25 μm spectral indices whereas this is true for only 20% of sources in the latter group.

indices whereas this is true for only 20% of sources in the latter group.

The difference between the spectral indices of the YSO candidates in the two groups may be related to the selection criteria (Sec. 3) used to identify the near-infrared counterparts. We have selected objects that appeared associated with nebulosity or that appeared to be very red, i.e., much brighter at K than at J. Figure 15 may indicate that red objects in the $(J-K)$ sense tend to be also red in the 12/25 μm sense. These objects would therefore tend to exhibit broadband spectral energy distributions that rise with increasing wavelengths, from 1 μm (J band) to at least 25 μm. A corollary of this may be that bluer 12/25 μm sources are bluer at near infrared, and thereby not easily distinguished from unrelated stars in our images.

Photometry of all the YSOs found will be presented in our final paper in this series (Yun & Clemens 1994b).

4.2 Objects Exhibiting Nebular Emission

In this section, we analyze the collective properties of the near-infrared counterparts found. We focus primarily on the 11 YSO candidates found to be associated with near-infrared nebulosities. We discuss the morphologies of the nebulae and explore the relationships with near-infrared and optical nebulosities, 12/25 μm spectral indices, and mass outflows.

4.2.1 Shapes and extents of the nebulosities

The near-infrared nebulosities present in the images generally contain a stellarlike source surrounded by an extended component. The nebula towards CB205 is clearly bipolar or biconical (Morris 1981), with a symmetric hourglass-like pattern. However, the nebula in CB205 is exceptional with no other similar nebula in our sample.

Models of embedded infrared nebulae have been computed by Lazareff *et al.* (1990), Whitney & Hartmann (1992), Whitney & Hartmann (1993), and Kenyon *et al.* (1993). We have attempted to match the appearances of our nebulae to the suite of infrared (even-numbered) models calculated by Whitney & Hartmann (1993; hereafter referred to as WH 93) in order to assess both the robustness of their models and to try to estimate the physical properties of our embedded sources and nebulae.

In particular, our mostly unresolved nebulae (CB3, CB31, and CB32) are well matched to two of the WH93 models (Nos. 4 and 16 with projection cosine values μ=0.6 or 0.9). Our nebulae showing one-dimensional features (CB54, CB60, CB188, and CB216) are most similar to WH93 model 12, again with projection cosines of 0.6 or 0.9. Our two-dimensional nebulae were individually matched as follows. CB205/L810 was very well described by WH93 model 8 in the edge-on (μ=0) configuration, with the caveat that the lobe opening angles of the CB205 nebula (~110°) exceed the model opening angle (~90°). Their model 8 consists of a small disk plus an infalling envelope with two symmetric conically shaped evacuated lobes. They did not experiment with varying the opening angle of their cavity, so we infer that while CB205 must have conical cavities similar to model 8, the cone opening angles must larger than the 30° half-angle used in the model.

CB230 in the J band appears closest to models 2(μ=0.6) and 8(μ=0.6), while the K-band image seems to favor model 8(μ=0.6) over model 2.

The common nebulosities containing double stars (CB52, CB54, CB60, CB230) were not well matched by the WH93 models, as expected, since they did not model multiple illumination sources.

Also, interestingly, the crescent-shaped CB6 nebula had no analog in the WH93 model suite. While uniconical nebulae were well modeled (e.g., CB230) by WH93, none of their models showed the strong depression in the central portion of the extended cone (which produces the distinct "banana" shape of the CB6 nebula).

With the exception of CB205, all of the nebulae which could be matched to the WH93 models tended to be asymmetric, and were matched to moderately (μ=0.6) to highly inclined (μ=0.9) models. A similar conclusion was reached by Kenyon *et al.* (1993) for infrared nebulae in the Taurus–Auriga cloud. Our more extended nebulae were also more readily modeled by infalling envelopes with biconical cavities (models 6, 8, 10) than by envelopes with no cavities or with evacuated central cylinders. However, the one-dimensional segments or arcs seemed to be only produced in the model envelopes with central cylindrical cavities (models 12, 14, 16).

The most general conclusion we draw from this comparison is that our own nebulae are well modeled as being due to scattered light from extincted central sources, and the nebulae are not self-luminous. This conclusion is strongest for the extended, well-resolved nebulae, and somewhat weaker for the partially unresolved one-dimensional nebulae.

4.2.2 Relationships to outflows

Several polarization studies (Hodapp 1984; Sato *et al.* 1985; Tamura & Sato 1989) have found that extended infrared nebulae associated with CO bipolar outflows often show polarization position angles oriented perpendicular to the outflow directions. Modeling by WH93 has shown that the polarization directions are governed by the nature of the scattering (generally single) and the geometry of the star, disk, and envelope combination.

We have shown evidence supporting the close relationship between infrared nebulae and CO bipolar outflows (Secs. *3.2.1*, *3.2.6*, *3.2.9*, *3.2.10*, and *3.2.11*). Some of our nebulae are sufficiently extended to allow a comparison of their morphologies with the morphologies of the CO outflow lobes. In these cases, there are good spatial coincidences between the location of the blue outflow lobes and the more extended parts of the infrared nebulae (CB54YC1, CB205YC1, CB230YC1). In addition, for the cases where nebular axes are evident (e.g., arc or segment nebulae), the direction of these axes are roughly parallel to the outflow axes (e.g., the nebulae and outflows towards CB205, CB216, CB230). We conclude that the nebulae seen in our images are reflection nebulae, and our results support the notion (Tamura *et al.* 1991b) and modeling (WH93) that these infrared reflection nebulae are good morphological tracers of CO mass outflow.

Next, we consider the group of four YSO candidates with multiple (binary) counterparts (CB52YC1, CB54YC1, CB60YC1, CB230YC1). CB52YC1 does not have an associated CO outflow. CB60YC1 was not searched for an outflow. Both of the other two YSO candidates, CB54YC1 and CB230YC1, have associated CO outflows. In both cases, the angle between the outflow axis and the binary axis is approximately 90°. Furthermore, the separations between the two stars seem to be similar (~12″, or ~7000 AU at 600 pc distance) for these two pairs of YSO candidates. However, at present we cannot assign the outflows seen to one or the other stars of each binary (Yun & Clemens 1994a).

4.2.3 Colors of the nebulae

Some remarkable facts stand out from an examination of Table 3. None of the three objects with nebulosities detected in the K and H bands, but not in J, show optical nebulosity on the Palomar prints. On these prints, these near-infrared objects are positioned in very opaque regions of the clouds, as judged by the strongly reduced number of stars seen in the POSS towards those regions. This strongly contrasts with the situation in the group of objects detected in the J and H bands, but not in K. In this group, three (CB31YC1, CB32YC1, and CB60YC1) out of four YSO candidates show optical nebulosities on the POSS prints.

Furthermore, the 11 objects in Table 3 exhibiting extended nebular emission seem to follow a simple rule: objects whose nebulosity is more conspicuous (brighter or more extended) in J than in K, have positive 12/25 μm spectral indices; objects whose nebulosity is more conspicuous in K than in J, have negative 12/25 μm spectral indices. This is illustrated in Fig. 16. This figure shows the cumulative fraction of sources with spectral indices smaller than or equal to a fixed value. The solid line refers to the group of objects whose nebulosity is brighter in J than in K; the dashed line refers to the group of objects whose nebulosity is brighter in K than in J (the separation between the two groups occurs roughly at $\Sigma_J - \Sigma_K \approx 1.5$ mag arcsec^{-2}, where Σ is the nebula surface brightness). There is clearly a separation between the two groups of objects: all of the objects with negative spectral indices have brighter K nebulosities and all of the objects with positive spectral indices have brighter J nebulosities.

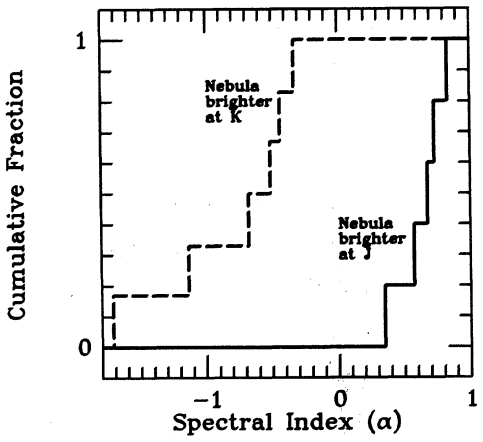

FIG. 16. Cumulative fraction of sources with spectral indices smaller than or equal to a fixed value. The solid line refers to the group of objects whose nebulosity is more conspicuous in J than in K; the dashed line refers to the group of objects whose nebulosity is more conspicuous in K than in J. There is clearly a separation between the two groups of objects, with all the objects with negative spectral indices having brighter K nebulosities and all objects with positive spectral indices having brighter J nebulosities.

These facts argue in favor of a more embedded nature for the YSOs with negative 12/25 μm spectral indices. In our sample of objects with near-infrared nebulosity, objects whose nebulosities are more conspicuous in K are associated with a lack of visible stars in the Palomar prints and with negative 12/25 μm spectral indices of their YSO candidates. Objects whose nebulosities are more conspicuous in J are associated with visible stars in the Palomar prints and with positive 12/25 μm YSO-candidate spectral indices. In addition, because shorter wavelength photons are more readily absorbed by the cloud than photons of longer wavelength, near-infrared nebulosity brighter in K than in J is likely to indicate that the origin of the emission lies behind more opaque cloud layers. For the same reason, the cases where the nebulous emission is seen strongest in the J band may correspond to light being scattered off regions in the cloud with smaller line-of-sight extinctions.

5. AN EVOLUTIONARY SEQUENCE?

We conclude that the 12/25 μm index for a YSO is a good predictor or indicator of the embeddedness of a YSO, and of the age of the YSO. As a consequence, the YSOs in Table 2, when ordered by increasing values of the 12/25 μm spectral indices, may constitute an evolutionary sequence, from younger objects with larger negative (red) spectral indices

TABLE 5. Near-infrared counterparts of YSO candidates in Bok Globules: Ordered by 12/25 μm spectral index.

YSO candidate	Spectral Index (12/25 μm)	Outflow detected	Infrared nebula brighter at K	Infrared nebula brighter at J	Palomar nebula or counterpart
(1)	(2)	(3)	(4)	(5)	(6)
CB214YC1	−1.88	√	...	...	...
CB6YC1	−1.43	...[a]	√	...	...
CB205YC1	−0.84	√	√	...	√
CB244YC1	−0.71	√	...	...	...
CB34YC1	−0.67	√	...	...	...
CB216YC1	−0.52	√	√	...	...
CB188YC1	−0.51	√	√	...	...
CB54YC1	−0.37	√	√	...	...
CB232YC1	−0.33	√	...	...	...
CB230YC1	−0.29	√	√	...	√
CB39YC1	−0.17	√	...	...	√
CB240YC1	−0.04	...[b]	...	...	...
CB32YC1	0.50	...	...	√	√
CB31YC1	0.65	...	...	√	√
CB60YC1	0.70	...[b]	...	√	√
CB52YC1	0.76	...	...	√	√
CB3YC1	0.90	...	...	√	√
CB142YC1	1.14	...	...	...	...
CB180YC1	1.21	...	...	...	...
CB128YC1	1.81	...	...	...	√

Notes to TABLE 5

[a] Vestiges of ^{12}CO molecular outflow in the contour map of the red wing integrated intensity.
[b] Not searched for molecular outflow.

and whose nebulosities are seen in the K band, to objects in later stages of the pre-main-sequence evolution with larger positive (bluer) spectral indices and whose scattered nebular emission is seen in the J band.

Table 5 offers evidence of such an evolutionary sequence. In this table, the 20 YSO candidates [column (1)] are listed by increasing values of their 12/25 μm spectral indices [column (2)]. For each of the YSO candidates, column (3) indicates whether a CO outflow was detected (Yun & Clemens 1992). Columns (4) and (5) indicate whether a near-infrared counterpart displaying nebulosity was found, and in which band (K or J) the nebulosity was brighter. Column (6) indicates whether there is a POSS stellar counterpart or nebulosity associated with each YSO candidate. Notice the concentration of check marks (√) in columns (3) and (4) for YSO candidates whose 12/25 μm spectral indices are negative. In contrast, notice the the concentration of check marks (√) in columns (5) and (6) for YSO candidates whose 12/25 μm spectral indices are positive. We conclude that negative 12/25 μm spectral indices, presence of outflows, bright K-band infrared nebulae, and absence of a POSS counterpart are indicators of earlier stages in the life of a pre-main-sequence low-mass star.

Theoretical modeling of broadband spectral energy distributions from young stars surrounded by disks exhibit similar traits (e.g., Adams *et al.* 1987; Marsh & Mahoney 1992). Younger systems exhibit energy distributions dominated by the outer, cooler portions of circumstellar accretion disks, while much older systems are dominated by stellar photospheric emission. In between these extremes, the details of the disk properties near the star affect the mid-infrared signature. Mid-infrared spectral gaps or dips are interpreted as physical gaps in the disk (Marsh & Mahoney 1992) or dust grain opacity effects (Boss & Yorke 1993).

In our sample, the correlation of negative 12/25 μm spectral indices with high-velocity outflows can be understood to signify significant disk accretion (driving the outflows) coupled with *no* midinfrared gap (negative 12/25 μm spectral indices). That the nonoutflow sources have generally positive 12/25 μm indices seems to be indicative of a reduced role for accretion for these young stars. A similar relation has been shown correlating the presence of T Tauri winds with optically thick disks (see the review by Edwards *et al.* 1993). There, inner disk opacity is indicated by the infrared $K-L$ color of the star. Our use of the 12/25 μm index will tend to probe the cooler, presumably more distant parts of the circumstellar disk.

Whether the cessation of the accretion phase is due to outflow or wind disruption of the inner disk (see Strom *et al.* 1993) or is related to close binary companions (Mathieu *et al.* 1991) is not known. Interestingly, our near-infrared survey has uncovered very wide binaries (10″–12″∼7000 AU), but no intermediate distance binaries. High-angular resolution imaging of the stellarlike sources in our sample may provide important information regarding their true binary distribution.

In our final paper in this series (Yun & Clemens 1994b), we will combine *IRAS* and near-infrared fluxes for our sources into broadband spectral energy distributions. Detailed examination of the disk properties and evolutionary states of these sources are to be found in that paper.

6. SUMMARY

(1) Thirty-four Bok globules have been imaged in the near-infrared JHK bands using state-of-the-art NICMOS 3 and SQIID cameras.

(2) Examination of the near-infrared images revealed that 20 globules show evidence of embedded nebulosity or very red stellar objects.

(3) The group of globules not showing evidence of nebulosity or very red stellar objects is characterized by YSO candidates with positive 12/25 μm spectral indices (bluer colors).

(4) Several possible binaries with separations of about 10 arcsec (CB52YC1, CB54YC1, CB60YC1, and CB230YC1) were found to reside in common infrared nebulosity.

(5) The morphologies of the nebulae found are well matched by theoretical models (WH93) consisting of a small disk plus an infalling envelope with evacuated cavities.

(6) Our results support the idea that infrared reflection nebulae, seen at 2.2 μm, are a good morphological tracer of CO mass outflow.

(7) The 12/25 μm index for a YSO candidate is a good indicator of the age of the YSO+ disk system.

(8) The group of objects displaying nebulosities seems to form an evolutionary sequence, from objects deeply embedded in the cloud (showing nebulosities mostly in the K band, having associated molecular outflows and no optical counterparts) to objects in a later stage of their pre-main-sequence evolution (showing nebulosity in the J band only, no detected molecular outflow, and having optical counterparts or optical nebulae).

REFERENCES

Adams, F. C., Lada, C. J., & Shu, F. H. 1987, ApJ, 312, 788
Bok, B. J., & Reilly, E. F. 1947, ApJ, 105, 255
Bok, B. J. 1978, PASP, 90, 489
Boss, A. P., & Yorke, H. W. 1993, ApJ, 411, L99
Buhrke, T., & Mundt, R. 1986, in Circumstellar Matter, IAU Symposium No. 122, edited by I. Appenzeller and C. Jordan (Reidel, Dordrecht), p. 175
Cabrit, S., Goldsmith, P. F., & Snell, R. L. 1988, ApJ, 334, 196
Cernicharo, J., Bachiller, R., & Duvert, G. 1985, A&A, 149, 273
Clemens, D. P., & Barvainis, R. E. 1988, ApJS, 68, 257
Clemens, D. P., Yun, J. L., & Heyer, M. H. 1991, ApJS, 75, 877
Dickman, R. L., & Clemens, D. P. 1983, ApJ, 271, 143
Duvert, G., Cernicharo, J., Bachiller, R., & Gómez-González, J. 1990, A&A, 233, 190
Edwards, S., Ray, T., & Mundt, R. 1993, in Protostars and Planets III, edited by E. Levy and J. Lunine (University of Arizona Press, Tucson), p. 567
Ellis, T., *et al.* 1992, Proceedings of the Society of Photo-Optical Instrumentation Engineers (in press)
Frerking, A. F., & Langer, W. D. 1982, ApJ, 256, 523
Frerking, A. F., Langer, W. D., & Wilson, R. W. 1987, ApJ, 313, 320
Goldsmith, P. F., Snell, R. J., Heyer, M. H., & Langer, W. D. 1984, ApJ, 286, 599
Graham, J. A. 1988, in Progress and Opportunities in Southern Hemisphere Optical Astronomy, edited by V. M. Blanco and M. M. Phillip, ASP Conference Series, p. 1
Hodapp, K. W. 1984, A&A, 141, 255
Keene, J., *et al.* 1983, ApJ, 274, L43
Kenyon, S. J., Whitney, B. A., Gomez, M., & Hartmann, L. 1993, ApJ, 414, 773
Lazareff, B., Pudritz, R. E., & Morin, J. L. 1990, ApJ, 358, 170
Leung, C. M., Kutner, M. L., & Mead, K. N. 1982, ApJ, 262, 583
Marsh, K. A., & Mahoney, M. J. 1992, ApJ, 395, L115
Mathieu, R. D., Adams, F., & Latham, D. W. 1991, AJ, 101, 2184
Moriarty-Schieven, G. H., & Snell, R. L. 1989, ApJ, 338, 952
Morris, M. 1981, ApJ, 249, 572
Neckel, T., & Staude, H. J. 1990, A&A, 231, 165
Ogura, K., & Hagesawa, T. 1983, PASJ, 35, 299
Reipurth, B. 1983, A&A, 117, 183
Reipurth, B., & Graham, J. A. 1988, A&A, 202, 219
Reipurth, B. 1991, The Physics of Star Formation and Early Stellar Evolution, edited by C. J. Lada and N. D. Kylafis (Reidel, Dordrecht), p. 497
Rieke, M. J., Montgomery, E. F., Rieke, G. H., Vural, K., Blessinger, M., & Kleinhans, W. 1989, Proceedings of the Third Infrared Detector Technology Workshop, edited by C. R. McCreight, p. 321
Sato, S., Nagata, T., Nakajima, T., Nishida, M., Tanaka, M., & Yamashita, T. 1985, ApJ, 291, 708
Scarrot, S. M., Rolph, C. D., & Tadhunter, C. N. 1991, MNRAS, 248, 27
Scappini, F., Caselli, P., & Palumbo, G. G. C. 1991, MNRAS, 249, 763
Strom, S. E., Edwards, S., & Skrutskie, M. F. 1993, in Protostars and Planets III, edited by E. Levy and J. Lunine (University of Arizona Press, Tucson), p. 837
Sugitani, K., Fukui, Y., Mizuno, A., & Ohashi, N. 1989, ApJ, 342, L87
Tamura, M., & Sato, S. 1989, AJ, 98, 1368
Tamura, M., Gatley, I., Waller, W., & Werner, M. W. 1991a, ApJ, 374, L25
Tamura, M., Gatley, I., Joyce, R. R., Ueno, M., Suto, H., & Sekiguchi, M. 1991b, ApJ, 376, 611
Thompson, R., *et al.* 1989, Proceedings of the Third Infrared Detector Technology Workshop, edited by C. R. McCreight, p. 331
Villere, K. R., & Black, D. C. 1980, ApJ, 236, 192
Whitney, B. A., & Hartmann, L. 1992, ApJ, 395, 529
Whitney, B. A., & Hartmann, L. 1993, ApJ, 402, 605 (WH93)
Young, J. S., Goldsmith, P. F., Langer, W. D., Wilson, R. W., & Carlson, E. R. 1982, ApJ, 261, 513
Yun, J. L. 1992, Ph.D thesis, Boston University
Yun, J. L., & Clemens, D. P. 1990, ApJ, 365, L73
Yun, J. L., & Clemens, D. P. 1992, ApJ, 385, L21
Yun, J. L., Clemens, D. P., McCaughrean, M., & Rieke, M. 1993, ApJ, 408, L101
Yun, J. L., & Clemens, D. P. 1994a, ApJS, 92, 145
Yun, J. L., & Clemens, D. P. 1994b, in preparation
Zinnecker, H. 1988, Formation and Evolution of Low-Mass Stars, edited by A. K. Dupree and M. T. V. T. Lago, (Reidel, Dordrecht), p. 111